3D Hand-Eye Calibration for Collaborative Robot Arm: Look at Robot Base Once

Leihui Li¹, Lixuepiao Wan¹, Volker Krueger² and Xuping Zhang^{1,*}

¹Department of Mechanical and Production Engineerin, Aarhus University, Denmark

²Department of Computer Science, Lund University, Lund, Sweden

Keywords: Hand-Eye Calibration, 3D Vision, Collaborative Robot, Robot Arm.

Abstract:

Hand-eye calibration is a common problem in the field of collaborative robotics, involving the determination of the transformation matrix between the visual sensor and the robot flange to enable vision-based robotic tasks. However, this process typically requires multiple movements of the robot arm and an external calibration object, making it both time-consuming and inconvenient, especially in scenarios where frequent recalibration is necessary. In this work, we extend our previous method which eliminates the need for external calibration objects such as a chessboard. We propose a generic dataset generation approach for point cloud registration, focusing on aligning the robot base point cloud with the scanned data. Furthermore, a more detailed simulation study is conducted involving several different collaborative robot arms, followed by real-world experiments in an industrial setting. Our improved method is simulated and evaluated using a total of 14 robotic arms from 9 different brands, including KUKA, Universal Robots, UFACTORY, and Franka Emika, all of which are widely used in the field of collaborative robotics. Physical experiments demonstrate that our extended approach achieves performance comparable to existing commercial hand-eye calibration solutions, while completing the entire calibration procedure in just a few seconds.

1 INTRODUCTION

3D vision systems, particularly those utilizing point cloud data, provide detailed geometric surface information that enables comprehensive spatial understanding (Munaro et al., 2016). This capability has significantly advanced modern manufacturing systems (Wang et al., 2021, 2017), especially in the fields of collaborative robot and automated operations (Robinson et al., 2023; Halme et al., 2018). Furthermore, the integration of perception sensors with robotic manipulators has greatly enhanced automation applications that require vision-based intelligent control and manipulation (Zhou et al., 2021b; Ten Pas et al., 2017; Zhou et al., 2021a). A fundamental problem in collaborative robot is establishing accurate coordination between the sensing system (eye) and the tool center point (hand) (Horaud and Dornaika, 1995; Jiang et al., 2022; Enebuse et al., 2021). This coordination, known as hand-eye calibration, determines the spatial transformation, which consists of both translation and rotation.

Calibration targets in conventional hand-eye calibration are essential components (Tsai et al., 1989; Strobl and Hirzinger, 2006), with checkerboards and circles being the most common standard patterns (Mallon and Whelan, 2007). By executing multiple collaborative robot arm movements while acquiring corresponding images, the homogeneous transform equation is constructed and solved to estimate the hand-eye transformation (Wang and Song, 2024). Such conventional target-based approaches have inherent limitations: mandatory manual integration of calibration targets, inevitably approximate solutions due to their nonconvex nature (Wu et al., 2020), and multiple robot movements for data collection that significantly increase time consumption (Zhou et al., 2023; Allegro et al., 2024; Ma et al., 2018).

To address challenges in traditional hand-eye cal-

used methodologies (Enebuse et al., 2021, 2022; Wijesoma et al., 1993) typically depend on specialized calibration equipment and complex procedures, creating practical limitations in dynamic industrial settings where systems require frequent recalibration. In this paper, we aim to achieve fast and effective hand-eye calibration through 3D vision.

^{*}Corresponding author

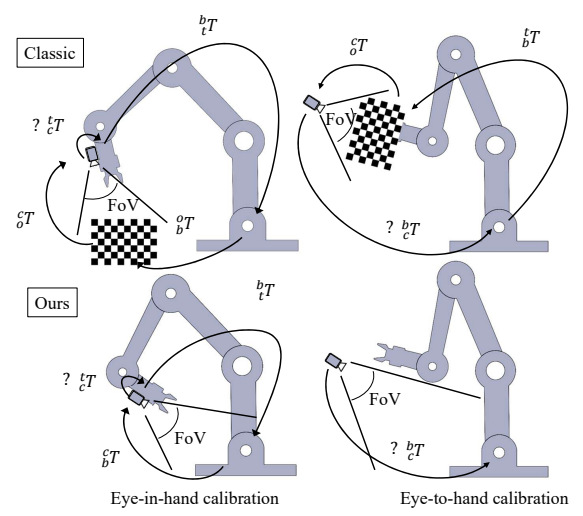


Figure 1: Our proposed hand-eye and the traditional calibration that needs the external calibration objects.

ibration, we build on our previous work (Li et al., 2024), which retains user-friendliness by eliminating additional calibration targets and using the robot base as a unified target, enabling rapid calibration. In this paper, a generic dataset generation method is proposed to make our approach applicable to a wide range of collaborative robots. Additionally, 14 robotic arms are used in the simulation to thoroughly evaluate the robustness and accuracy of our method, demonstrating its feasibility. Finally, a physical experiment compares our method with a commercial hand-eye calibration solution, demonstrating its practical applicability.

Our main contributions are as follows:

- 1. We improve and develop a generic dataset generation method: in addition to capturing point clouds around the robot base on hemispheres with varying radii, we also simulate realistic robot poses by exploring diverse joint angle combinations.
- A total of 14 collaborative robot arms from 9 brands are included in our study, each contributing 900 hand-eye calibration results. Individual and aggregated results are analyzed, demonstrating the approach's generalizability.
- Real-world experiments are conducted in an industrial setting, where our proposed method is compared with a commercial calibration setup. Our method is validated using both single and multiple joint configurations, demonstrating its effectiveness and comparable performance.

2 RELATED WORK

Hand-eye calibration is a prerequisite for vision-guided robotic manipulation systems using collaborative robot arms (Hong and Ha, 2025), and the accuracy of this calibration fundamentally determines the subsequent precision of vision-based control and manipulation within the system. To compute the unknown transformation between a robot end-effector and a camera, the methodological approaches to addressing hand-eye calibration can be categorized into (Enebuse et al., 2021): solving homogeneous transform equations, reprojection error minimization techniques, and learning-based methods.

The conventional equation formulations can be represented as (Zhu et al., 2024):AX = XB (Shiu and Ahmad, 1987) or AX = YB (Zhuang et al., 1994). The former approach determines the hand-eye matrix X through multiple sets of robot movements. To eliminate error propagation inherent in this formulation and improve noise sensitivity, Zhuang and Shiu (Zuang and Shiu, 1993) proposed a sequential method for solving matrix X. Recently, Ma et al. (Ma et al., 2016) proposed novel probabilistic approaches that extend the Batch method to filter outlier data. The second equation seeks to simultaneously determine both the hand-eye matrix X and the transformation matrix Y from the robot base to the world coordinate. To solve this equation, many solution strategies utilize linear least-squares minimization combined with iterative optimization schemes (Tabb and Ahmad Yousef, 2017). In response to these approaches, Ha (Ha, 2022) proposed a probabilistic framework that elucidates the ambiguous aspects of existing methods by revealing their underlying assumptions about system noise. An alternative approach leverages reprojection error minimization for hand-eye calibration. Based on this principle, Kenji and Emanuele (Koide and Menegatti, 2019) proposed a hand-eye calibration method that minimizes reprojection error via pose graph optimization, allowing robust estimation across various camera models. However, these conventional methods and their derivative approaches typically require either multiple robot movements (at least two), additional calibration targets, or suffer from high algorithmic complexity and extended computational time.

To overcome the limitations of conventional approaches, learning-based methodologies have been progressively incorporated into hand-eye calibration procedures. Hua and Zeng (Hua and Zeng, 2021) established coordinate transformation relationships through neural network training, achieving enhanced grasping accuracy even under the influence of noise

perturbations. In constrained surgical scenarios, Krittin et al. (Pachtrachai et al., 2021) estimated hand-eye transformation through a deep convolutional network, leveraging temporal information between frames and kinematic data without requiring calibration objects. Bahadir et al. (Bahadir et al., 2024) proposed Continual Learning-based approaches that enable progressive extension of the calibration space without complete retraining, while accommodating changes in camera pose over time. Nevertheless, existing learning-based methods still present considerable room for improvement. The associated neural networks exhibit high computational complexity, limited generalizability for straightforward implementation in common robotic manipulators, and in some cases, continued dependence on external calibration objects. Furthermore, some approaches are limited to either eye-in-hand or eye-to-hand calibration, failing to address both scenarios.

In comparison with the aforementioned methodologies, our proposed method maintains the advantage of calibration-object-free operation while accommodating both eye-in-hand and eye-to-hand calibration configurations. By looking at the robot base, a closed kinematic chain is established, allowing the transformation matrix between the camera and the robot flange to be determined straightforwardly. In addition, we introduce a dataset generation method for point cloud registration of the robot base, enhancing the generality of our approach. Simulations involving 14 commonly used collaborative robot arms, along with physical experiments comparing our method to commercial solutions, demonstrate the applicability and effectiveness of the proposed method.

3 PROBLEM DEFINITION AND METHODS

In vision-guided collaborative robot systems, handeye calibration aims to determine the transformation between the camera and the tool center point (eye-inhand) or the robot base (eye-to-hand). In eye-in-hand calibration, the camera is mounted on the robot's endeffector, moving with the arm. In contrast, in eye-tohand calibration, the camera is fixed in the environment to observe the robot's workspace. To formalize this, we define the coordinate systems: the robot base as F_b , the tool center point as F_t , calibration object as F_o , and the camera as F_c .

3.1 Eye-in-Hand Calibration

In the eye-in-hand configuration, the camera is rigidly mounted on the robot's flange, as illustrated in the first one in Figure 1. The primary objective is to compute the rigid transformation matrix between the camera coordinate system and the tool center point (TCP) frame. This problem is commonly formulated as AX = XB, where X represents the transformation to be solved. This calibration typically requires the robot to move to multiple poses while observing a calibration target. Specifically, it can be expressed as

$${}_{t}^{b}\mathbf{T}_{i}^{-1}{}_{t}^{b}\mathbf{T}_{jc}^{t}\mathbf{T} = {}_{c}^{t}\mathbf{T}_{o}^{c}\mathbf{T}_{io}^{c}\mathbf{T}_{j}^{-1}$$

$$(1)$$

where i and j denote two distinct robot poses from the set of calibration measurements, and ${}^b_t \mathbf{T}$ represents the transformation matrix from the frame of the tool center point to the robot base coordinate system. ${}^b_t \mathbf{T}$ can be computed through forward kinematics, ${}^c_t \mathbf{T}$ is the unknown hand-eye transformation matrix to be determined, and ${}^o_o \mathbf{T}$ denotes the transformation from the calibration object frame to the camera frame.

3.2 Eye-to-Hand Calibration

In the eye-to-hand configuration, the camera is mounted at a fixed position within the workspace, external to the robot arm. This setup allows the camera to maintain a static, global viewpoint while the robot manipulator performs its movements. The primary objective of eye-to-hand calibration is to determine the rigid transformation matrix between the camera coordinate system and the robot base coordinate system. Through multiple movements of the calibration board at the robot arm's end-effector, the mathematical relationship can be established:

$${}_{b}^{t}\mathbf{T}_{i}^{-1}{}_{b}^{t}\mathbf{T}_{ic}^{b}\mathbf{T} = {}_{c}^{b}\mathbf{T}_{o}^{c}\mathbf{T}_{io}^{c}\mathbf{T}_{i}^{-1}$$
 (2)

where ${}_{c}^{b}\mathbf{T}$ is the unknown transformation from the camera coordinate system to the robot base coordinate system to be calculated, and ${}_{o}^{c}\mathbf{T}$ denotes the transformation from the camera frame to the observed calibration target, measured at different robot poses.

3.3 Look at Robot Base Once

The proposed methodology eliminates the need for a dedicated calibration object by directly observing the robot base, as illustrated in the second setup in Figure 1. Given the 3D data of the robot base, its 6D pose can be estimated, allowing the determination of the transformation matrix between the camera coordinate

system and the robot base coordinate system. This approach can be further extended to compute the transformation matrix between the TCP coordinate system and the camera coordinate system.

Given the captured robot base point cloud P = $\{p_i \in \mathbb{R}^3 | i = 1...n\}$ and the reference model point cloud $Q = \{q_j \in \mathbb{R}^3 | j = 1...m\}$, the objective of registration is to find the optimal rigid body transformation parameters: an orthogonal rotation matrix $R \in SO(3)$ and translation vector $t \in \mathbb{R}^3$ that minimize the error between the transformed actual point cloud and the reference model point cloud. The optimization objective can be expressed as

$$\min_{R,t} \sum_{i=1}^{n} \min_{j=1}^{m} \|p_i - (Rq_j + t)\|_2$$
 (3)

where $||p_i - (Rq_j + t)||_2$ is the Euclidean distance between the acquired point cloud and the reference point cloud of robot base. Due to a scale mismatch between the reference model and the acquired data, a pretransformation of the reference data, denoted $_{ref}^{ref'}$ **T**, is applied. The registration module provides the transformation $\frac{c}{r_e f'}$ **T**, leading to the formulation in Eq. 4.

$${}_{ref}^{c}\mathbf{T} = {}_{ref}^{c}{}_{T} \mathbf{T} \qquad (4)$$

$${}_{c}^{b}\mathbf{T} = {}_{ref}^{c}\mathbf{T}^{-1} \qquad (5)$$

$${}_{c}^{b}\mathbf{T} = {}_{ref}^{c}\mathbf{T}^{-1} \tag{5}$$

Here, the frame of the reference data is aligned with the frame of the robot base in the real world, which gives Eq. 5. For eye-in-hand calibration, each movement forms a closed kinematic chain as

$$\mathbf{I} = {}^{b}_{t} \mathbf{T} {}^{c}_{c} \mathbf{T} {}^{c}_{b} \mathbf{T} \tag{6}$$

The transformation matrix ${}_{c}^{t}\mathbf{T}$ therefore can be obtained by performing the transformation as

$${}_{c}^{t}\mathbf{T} = {}_{t}^{b}\mathbf{T}^{-1} {}_{b}^{c}\mathbf{T}^{-1} \tag{7}$$

The eye-in-hand setup is more computationally challenging due to the moving camera frame, whereas in eye-to-hand calibration, ${}^b_c\mathbf{T}$ can be estimated straightforwardly using a point cloud registration module. Therefore, we adopt the eye-in-hand configuration for experimental validation to demonstrate the robustness of our approach.

The main challenge lies in generating a dataset of robot base point clouds for registration training, where both the source data (captured point clouds) and the target data (reference model) are represented as point clouds. We begin by capturing the robot base through simulated 3D camera views positioned around a sampled hemisphere centered at the base origin. Additionally, to enhance realism, we augment the dataset by simulating valid robot poses based on joint constraints, reflecting realistic configurations seen in actual applications. Both datasets are used for training the point cloud registration network.

The flowchart of our proposed method is illustrated in Figure 2, where the first step involves moving the robot arm to position the robot base within the camera's field of view. Given the ${}_{h}^{c}\mathbf{T}$, which can be estimated by the point cloud registration module, and ${}_{t}^{b}\mathbf{T}$, provided by forward kinematics, the ${}_{c}^{t}\mathbf{T}$ can finally be estimated as the result of the hand-eye calibration.

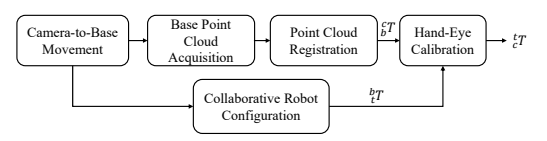


Figure 2: Flowchart of the developed hand-eye calibration.

EXPERIMENTS

Preparation and Experiment Setup

The robot arms used in our simulation environment are listed in Table 2. We utilize PyBullet as the simulation platform, where the robot arm is represented in URDF and OBJ file formats for loading and generating the trainable dataset. PREDATOR (Huang et al., 2021), a registration network designed for lowoverlap point clouds, is adopted in our study, followed by an ICP refinement step. This combination, as shown in our previous work (Li et al., 2024), improves robustness under partial overlap between the captured data and the robot base reference model.

In our study, the raw point clouds are used without background filtering. The camera is positioned on a virtual hemisphere with radii of 0.5 and 0.7 meters, capturing data from multiple perspectives to simulate real 3D camera acquisition. The final dataset, available online, which is combined with realistic simulated acquisition data, is used for training and is detailed in Table 1. Five random transformation matrices are applied to the captured data, and the point clouds are downsampled with a 2 mm voxel size.

Table 1: The size of the dataset for registration training.

FR3	Gen3	iiwa 7	iiwa 14	CRX -10iA	CRX -5iA	UR10e
1224	1074	810	954	1230	1026	816
UR5e	xArm6	xArm7	CRB 15000	HC10	EC66	EC63
1110	756	1140	768	1104	1014	1140

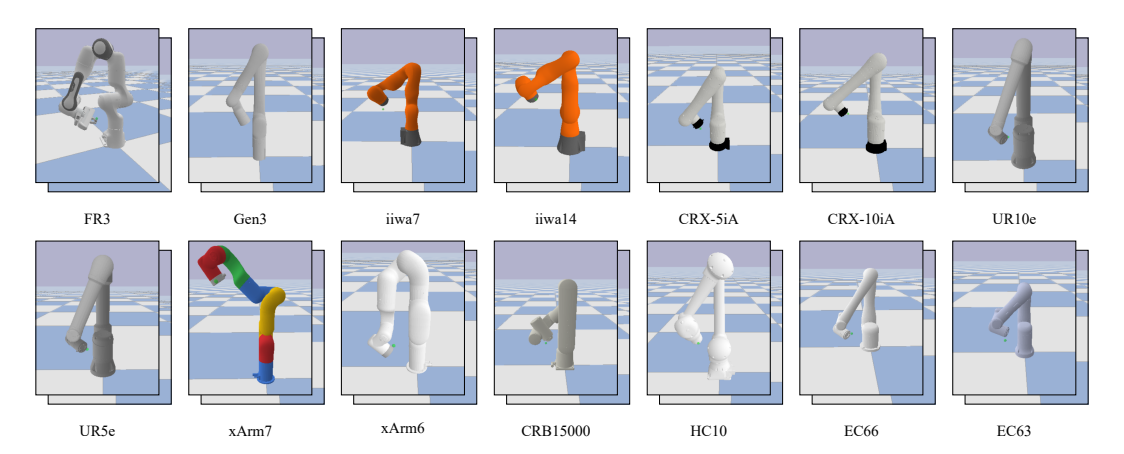


Figure 3: Visualization of randomly selected robot base-looking poses for various robotic manipulators, with one representative joint configuration shown.

as

Table 2: The collaborative robot arm used in our study.

Index	Robot Arm	Manufacturer	
1	FR3	Franka Robotics	
2	Gen3	Kinova	
3	iiwa 7	KUKA	
4	iiwa 14	KUKA	
5	CRX-5iA	FANUC	
6	CRX-10iA	FANUC	
7	UR10e	Universal Robots	
8	UR5e	Universal Robots	
9	xArm6	UFACTORY	
10	xArm7	UFACTORY	
11	CRB 15000	ABB	
12	HC10	Yaskawa Motoma	
13	EC66	Elite Robots	
14	EC63	Elite Robots	

4.2 Experimental Results

We evaluate the proposed approach in simulation, where the ground-truth transformation between the camera and TCP frame is known. For each robot arm, 30 random poses are generated within realistic joint angle limits to ensure kinematic feasibility, where the camera looks at the robot base and the joint rotations differ by at least 20 degrees to avoid near-duplicate configurations, as shown in Figure. 3. In all selected poses, the robot base remains within the camera's field of view to satisfy the method's requirements. At each pose, the end-effector-mounted 3D camera captures multiple base scans, each yielding an individual calibration result.

The final calibration result is obtained by averaging the rotation matrices in quaternion space and the translation vectors in Euclidean space. Ideally, the hand-eye calibration results obtained from the poses match the ground truth $(\bar{\bf R}$ and $\bar{\bf t})$, meaning the RTE and RRE in translation and rotation should be zero,

$$RTE = \|\mathbf{t} - \overline{\mathbf{t}}\|_2 \tag{8}$$

$$RRE = \arccos\left(\frac{\operatorname{trace}(\mathbf{R}^T \bar{\mathbf{R}}) - 1}{2}\right) \tag{9}$$

In addition to 30 unique base-looking poses for each robotic arm, we captured 30 repeated scans per pose, resulting in 900 calibration results per robot. The calibration performance across all robot arms is analyzed. As shown in Figure 4, it illustrates the average deviations in position and rotation errors, and reports the median and standard deviation for each robot. According to the results, the positional deviation for all poses remains below approximately 1.5 mm, and most rotational deviations are under 0.5°. The largest deviation is observed in the Gen3 robot arm. Overall, considering the point cloud voxel size of 2 mm, the tested poses yield reliable calibration performance, with a mean error of 1.29 mm in position and 0.39° in rotation.

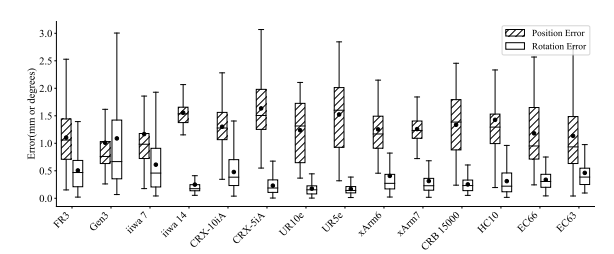


Figure 4: The hand-eye calibration results calculated from all poses for each robot arm are shown, with the mean value represented by a black dot. In the box plot, the horizontal line indicates the median value, while the top and bottom edges represent the standard deviation.

At each pose, 30 sets of 3D data from the robot base are collected, resulting in 30 calibration results. The deviation of different poses is shown in Figure.

5. According to the results, the positional deviation for each pose ranges from 1 mm to 1.6 mm, with the largest variation observed in robot CRX-5iA. The rotational deviation ranges from 0.16° to 1°, with the highest occurring in the Gen3 robot. The results indicate that, for the tested robot arm with different poses, the proposed method generally achieves a similar level of accuracy; that is, our method does not rely on any specific pose of the robot arm.

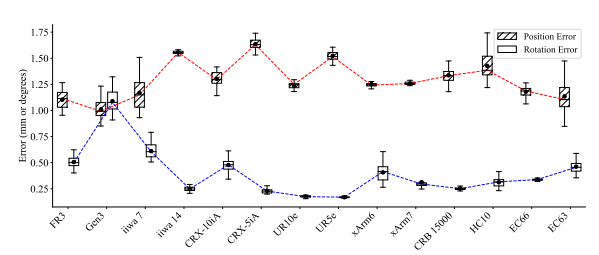


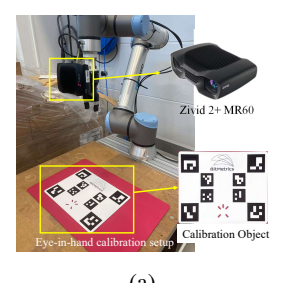
Figure 5: The differences between poses are illustrated by data points connected with red and blue lines, representing positional and rotational deviations, respectively.

This deviation, observed in the simulation environment, primarily arises from registration errors and the density of the point clouds, including both the retrieved data and the standard model. However, in real-world applications, additional factors such as camera imaging inaccuracies, point cloud noise, and discrepancies between the CAD model and the scanned robot base can further contribute to calibration errors. Therefore, real-world experiments are conducted to compare our proposed method with current commercial and mature solutions.

4.3 Real-World Experiments

The experiment is conducted on the UR10e robot with a high-accuracy 3D camera, the Zivid 2+ MR60, which achieves a spatial resolution of 0.24 mm at a working distance of 60 cm and generates highly detailed point clouds with a density of 5,000 points per cm². Although a high-precision 3D camera was used for real-world validation, the method is sensoragnostic and applicable to other 3D cameras capable of capturing the robot base geometry. The experimental setup is shown in Figure. 6a, where a calibration board is needed. Figure. 6b illustrates the calibration setup, with the camera oriented toward the robot base.

We compared our method with the current commercial eye-in-hand calibration solution, $BM\text{-HEC}^1$, which is based on the AX = XB formulation. The traditional calibration process was repeated four times, as shown in Figure 7, where multiple robot movements are required during each calibration. Our



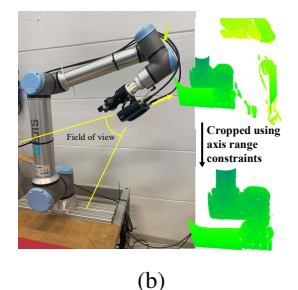


Figure 6: (a) Traditional calibration with external object and multiple robot movements. (b) Our calibration focusing on the robot base without external object.

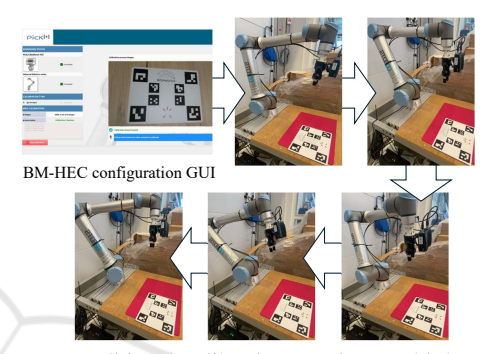


Figure 7: Traditional calibration requires multiple movements to capture the calibration object from different perspectives.

method was also performed four times, with each individual scan producing a complete calibration result. The calibration process typically takes an average of 2 minutes and 48 seconds, requiring 14 poses and images of the calibration board placed on the table. In contrast, our method completes the calibration in just a few seconds with a single pose. The average calibration results, i.e., the rigid relationship between the robot flange and the camera frame, are shown in Table 3, where the rotation in Euler space and position in Euclidean space are provided.

Table 3: Comparison of Eye-in-Hand Calibration with a Commercial Calibration Solution.

Method	TX (m)	TY (m)	TZ (m)	Time
BM-HEC	-0.054	-0.094	0.127	2m48s /
Ours	-0.051	-0.096	0.125	per calib
Method	RX (rad)	RY (rad)	RZ (rad)	Time
BM-HEC	0.013	0.044	0.017	6s /
Ours	0.014	0.044	0.019	per calib

According to the results in Table 3, The offsets between our method and BM-HEC are 3 mm, 2 mm, and 3 mm in terms of position, and 0.001 and 0.002 in rotation along the X and Z axes, respectively. The offset along the Y-axis is nearly zero. Most importantly, the calibration time of our proposed method is within 6 seconds, whereas the traditional method takes over

¹www.bitmetrics.es



Figure 9: Different poses used in our proposed hand-eye calibration method.

2.5 minutes, requiring multiple robot movements and a physical external calibration object.

Furthermore, given a single pose with multiple frames captured at that pose, calibration is computed multiple times. The results are shown in Figure. 10, where the average of the first N result(s) is presented for N = 1, 2, 5, 8, and 10. The results demonstrate that the largest translation deviation along the X-axis is approximately 0.2 mm, and the rotational deviation around the Y-axis is about 3×10^{-4} radians (0.019°) . Given a standard deviation of approximately 0.1×10^{-3} , using additional frames results in nearly identical calibration performance. Therefore, our method can reliably perform hand-eye calibration using just a single frame of 3D point cloud data.

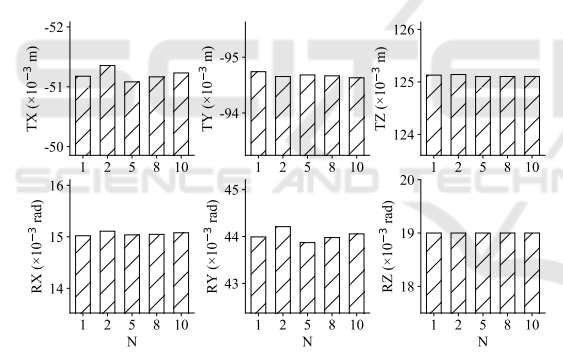


Figure 10: Average of the first n calibrations at a single pose.

In addition, different poses for eye-in-hand calibration on the UR10e, as illustrated in Figure 9, are validated. The results in Figure 11 show the maximum translation deviation was about 1.8 mm and the minimum about 0.6 mm, with rotation deviations between 0.001 and 0.002 radians. These results demonstrate that our proposed calibration method maintains consistent performance across multiple poses. Together with the large-scale evaluation on 14 collaborative robot models from 9 brands in simulation, this confirms the robustness and applicability of the method across diverse platforms.

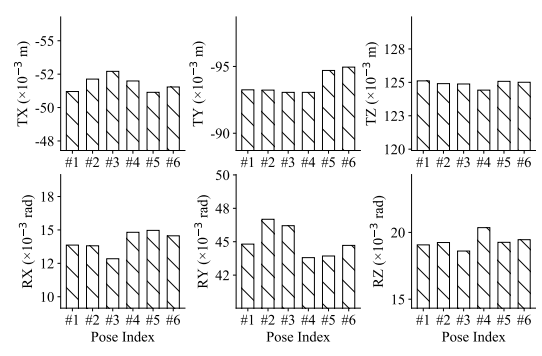


Figure 11: Hand-eye calibration results across 6 poses.

5 CONCLUSION AND FUTURE WORK

In this work, we extended and improved our previous method, a 3D vision-based hand-eye calibration approach. Our learning-based framework estimates the pose of the robot base, enabling the computation of the transformation matrix between the robot flange and the camera within seconds. We enhance the registration dataset by incorporating captured point clouds from diverse perspectives and realistic robot arm configurations. We conduct large-scale evaluations involving 14 collaborative robot models from 9 brands, including KUKA, ABB, and FANUC, and real-world validation with a high-precision 3D camera on an industrial-grade robot. These experiments confirm that our approach matches the calibration accuracy of commercial solutions, while greatly reducing calibration time and eliminating the need for external objects, making it broadly applicable to diverse collaborative robot systems.

In future work, we will focus on enhancing usability and long-term stability to further support deployment in diverse industrial environments.

ACKNOWLEDGMENTS

The authors thank Jialong Li for his excellent collaboration and patient support, everyone in RobotLab

LTH for their valuable assistance, and Jungner Company for its support.

REFERENCES

- Allegro, D., Terreran, M., and Ghidoni, S. (2024). Multicamera hand-eye calibration for human-robot collaboration in industrial robotic workcells. *arXiv* preprint *arXiv*:2406.11392.
- Bahadir, O., Siebert, J. P., and Aragon-Camarasa, G. (2024). Continual learning approaches to hand–eye calibration in robots. *Machine Vision and Applications*, 35(4):97.
- Enebuse, I., Foo, M., Ibrahim, B. S. K. K., Ahmed, H., Supmak, F., and Eyobu, O. S. (2021). A comparative review of hand-eye calibration techniques for vision guided robots. *IEEE Access*, 9:113143–113155.
- Enebuse, I., Ibrahim, B. K. K., Foo, M., Matharu, R. S., and Ahmed, H. (2022). Accuracy evaluation of hand-eye calibration techniques for vision-guided robots. *Plos one*, 17(10):e0273261.
- Ha, J. (2022). Probabilistic framework for hand–eye and robot–world calibration ax = yb. *IEEE Transactions on Robotics*, 39(2):1196–1211.
- Halme, R.-J., Lanz, M., Kämäräinen, J., Pieters, R., Latokartano, J., and Hietanen, A. (2018). Review of vision-based safety systems for human-robot collaboration. *Procedia Cirp*, 72:111–116.
- Hong, I. and Ha, J. (2025). Generative adversarial networks for solving hand-eye calibration without data correspondence. *IEEE Robotics and Automation Letters*.
- Horaud, R. and Dornaika, F. (1995). Hand-eye calibration. *The international journal of robotics research*, 14(3):195–210.
- Hua, J. and Zeng, L. (2021). Hand–eye calibration algorithm based on an optimized neural network. In *Actuators*, volume 10, page 85. MDPI.
- Huang, S., Gojcic, Z., Usvyatsov, M., Wieser, A., and Schindler, K. (2021). Predator: Registration of 3d point clouds with low overlap. In Proceedings of the IEEE/CVF Conference on computer vision and pattern recognition, pages 4267–4276.
- Jiang, J., Luo, X., Luo, Q., Qiao, L., and Li, M. (2022). An overview of hand-eye calibration. The International Journal of Advanced Manufacturing Technology, 119(1):77–97.
- Koide, K. and Menegatti, E. (2019). General hand–eye calibration based on reprojection error minimization. *IEEE Robotics and Automation Letters*, 4(2):1021– 1028
- Li, L., Yang, X., Wang, R., and Zhang, X. (2024). Automatic robot hand-eye calibration enabled by learning-based 3d vision. *Journal of Intelligent & Robotic Systems*, 110(3):130.
- Ma, L., Bazzoli, P., Sammons, P. M., Landers, R. G., and Bristow, D. A. (2018). Modeling and calibration of high-order joint-dependent kinematic errors for indus-

- trial robots. *Robotics and Computer-Integrated Manufacturing*, 50:153–167.
- Ma, Q., Li, H., and Chirikjian, G. S. (2016). New probabilistic approaches to the ax= xb hand-eye calibration without correspondence. In 2016 IEEE international conference on robotics and automation (ICRA), pages 4365–4371. IEEE.
- Mallon, J. and Whelan, P. F. (2007). Which pattern? biasing aspects of planar calibration patterns and detection methods. *Pattern recognition letters*, 28(8):921–930.
- Munaro, M., Rusu, R. B., and Menegatti, E. (2016). 3d robot perception with point cloud library.
- Pachtrachai, K., Vasconcelos, F., Edwards, P., and Stoyanov, D. (2021). Learning to calibrate-estimating the hand-eye transformation without calibration objects. *IEEE Robotics and Automation Letters*, 6(4):7309–7316.
- Robinson, N., Tidd, B., Campbell, D., Kulić, D., and Corke, P. (2023). Robotic vision for human-robot interaction and collaboration: A survey and systematic review. *ACM Transactions on Human-Robot Interaction*, 12(1):1–66.
- Shiu, Y. C. and Ahmad, S. (1987). Calibration of wrist-mounted robotic sensors by solving homogeneous transform equations of the form ax= xb.
- Strobl, K. H. and Hirzinger, G. (2006). Optimal hand-eye calibration. In 2006 IEEE/RSJ international conference on intelligent robots and systems, pages 4647–4653 IEEE.
- Tabb, A. and Ahmad Yousef, K. M. (2017). Solving the robot-world hand-eye (s) calibration problem with iterative methods. *Machine Vision and Applications*, 28(5):569–590.
- Ten Pas, A., Gualtieri, M., Saenko, K., and Platt, R. (2017). Grasp pose detection in point clouds. *The International Journal of Robotics Research*, 36(13-14):1455–1473
- Tsai, R. Y., Lenz, R. K., et al. (1989). A new technique for fully autonomous and efficient 3 d robotics hand/eye calibration. *IEEE Transactions on robotics and automation*, 5(3):345–358.
- Wang, G., Li, W., Jiang, C., Zhu, D., Li, Z., Xu, W., Zhao, H., and Ding, H. (2021). Trajectory planning and optimization for robotic machining based on measured point cloud. *IEEE transactions on robotics*, 38(3):1621–1637.
- Wang, X. and Song, H. (2024). One-step solving the handeye calibration by dual kronecker product. *Journal of Mechanisms and Robotics*, 16(10).
- Wang, X. V., Wang, L., Mohammed, A., and Givehchi, M. (2017). Ubiquitous manufacturing system based on cloud: A robotics application. *Robotics and Computer-Integrated Manufacturing*, 45:116–125.
- Wijesoma, S., Wolfe, D., and Richards, R. (1993). Eyeto-hand coordination for vision-guided robot control applications. *The International Journal of Robotics Research*, 12(1):65–78.
- Wu, J., Liu, M., Zhu, Y., Zou, Z., Dai, M.-Z., Zhang, C., Jiang, Y., and Li, C. (2020). Globally optimal sym-

- bolic hand-eye calibration. *IEEE/ASME Transactions* on Mechatronics, 26(3):1369–1379.
- Zhou, P., Peng, R., Xu, M., Wu, V., and Navarro-Alarcon, D. (2021a). Path planning with automatic seam extraction over point cloud models for robotic arc welding. *IEEE robotics and automation letters*, 6(3):5002– 5009.
- Zhou, Z., Li, L., Wang, R., and Zhang, X. (2021b). Deep learning on 3d object detection for automatic plug-in charging using a mobile manipulator. In 2021 IEEE International Conference on Robotics and Automation (ICRA), pages 4148–4154. IEEE.
- Zhou, Z., Ma, L., Liu, X., Cao, Z., and Yu, J. (2023). Simultaneously calibration of multi hand—eye robot system based on graph. *IEEE Transactions on Industrial Electronics*, 71(5):5010–5020.
- Zhu, D., Wu, H., Ding, T., and Hua, L. (2024). Point cloud registration-enabled globally optimal hand–eye calibration. *IEEE/ASME Transactions on Mechatronics*.
- Zhuang, H., Roth, Z. S., and Sudhakar, R. (1994). Simultaneous robot/world and tool/flange calibration by solving homogeneous transformation equations of the form ax= yb. *IEEE Transactions on Robotics and Automation*, 10(4):549–554.
- Zuang, H. and Shiu, Y. C. (1993). A noise-tolerant algorithm for robotic hand-eye calibration with or without sensor orientation measurement. *IEEE transactions on systems, man, and cybernetics*, 23(4):1168–1175.